Searching for gravitational waves from the coalescence of high mass black hole binaries

Author: Lau Ka Tung[1]
Mentors: Surabhi Sachdev[2], Tjonnie Li[2], Kent Blackburn[2], Alan Weinstein[2]

[1]Department of Physics, The Chinese University of Hong Kong, Shatin, New Territories, Hong Kong, China

[2]LIGO Laboratory, California Institute of Technology, Pasadena, California 91125, US

July 6, 2015

First Progress Report
Program: LIGO SURF 2015
Final version
DCC Number:

Abstract

The coalescence of high mass black hole binary is a possible source of gravitational waves which can be detected by the ground-based gravitational wave detectors. The frequency of the gravitational waves generated from the coalescence of compact binary lie on the aLIGO frequency band. The LIGO Scientific Collaboration uses search pipeline to search the coalescence signals from the detector output. The search pipeline uses matched filtering method to compute the signal-to-noise ratio (SNR) of the output with different templates in the template bank. The trigger identified using SNR is not sufficient to be confirmed as a gravitational wave signal since the existence of non-Gaussian noise (glitches) in the detector. The χ^2 veto is computed for the candidates to reject the false alarm. In this project, we will use the technique of machine learning to reduce the false alarm rate, in order that the sensitivity of the search pipeline can be improved. A large numbers of simulated background noise and true signals will be injected into the search pipeline, the final output of pipeline of each injection signal becomes the training set for machine learning. The learning will come up with a model for classifying the signals and glitches using the output of pipeline. The sensitivity of the search pipeline can be improved by suppressing the noise in the trigger candidates.

1 Graviational waves

General Relativity predicts the existence of gravitational waves. The change in gravitational fields produces ripples of curvature of spacetime, gravitational waves carry out energy away from the source and propagate at speed of light. When a gravitational wave passes through, it causes stretching and squeezing between test masses. We have not detected the stretching and squeezing effect from gravitational waves directly, but we have indirect evidence for the existence of gravitational waves[5].

In 1974, Joseph Taylor and Russell Hulse discovered the first binary pulsar. The binary consists of a neutron star and a pulsar, the pulsar emits electromagnetic pulse regularly towards the Earth. After more than a decade observation, Taylor and Hulse discovered an orbital decay from the shortening of the period of the pulse. The energy loss of the binary pulsar matches the loss due to gravitational radiation. This provides an evidence for the existence of gravitational waves.

2 Laser Interferometer Gravitational-wave Observatory (LIGO)

Laser Interferometer Gravitational-wave Observatory (LIGO) aims to detect the stretching and squeezing effect from gravitational waves directly. LIGO is a Michelson interferometer which can detect a small change between two arms. A laser beam is emitted to the beam splitter and split the light to the two arms. If two arms have the same length, then the light bounces back to the splitter with a destructive interference, and therefore, no light will be detected by the photosensor. However, if there is a gravitational wave passing through the detector and causes a length difference between two arms, some light can travel to the photosensor and the gravitational wave signal is detected.

In the operation of initial LIGO (iLIGO), no gravitational waves were detected. After a five years upgrade, Advance LIGO (aLIGO) is planned to begin a science run in late 2015. The sensitive of aLIGO is expected to be improved by 10 times with respect to iLIGO.

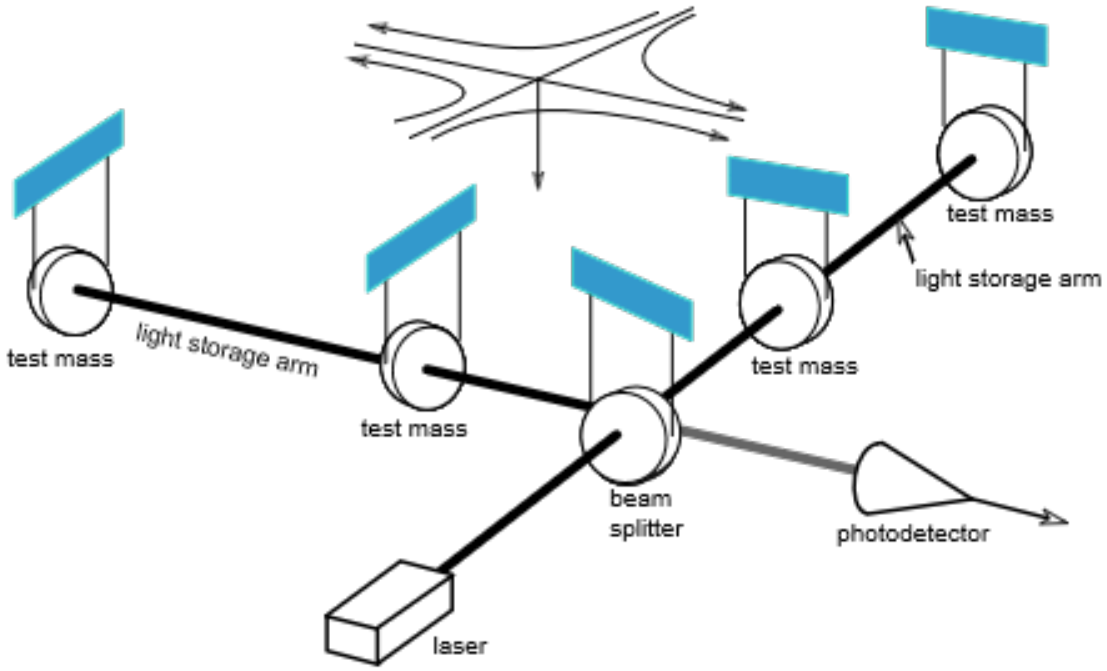

Figure 1: Laser interferometer.[1] A simplified schematic of a LIGO interferometer.

3 Compact binary coalescence

The frequency band of LIGO is about 10Hz - 10^3Hz. The frequency of gravitational waves from the coalescence of compact binary, such as binary neutron star, binary black hole and neutron star black hole binary, lies in the frequency band of LIGO, we expect to detect the gravitational wave signals from this astronomical process. Coalescence consists of three stages, which is known as inspiral, merger and ringdown. When the gravitational waves carry away energy and angular momentum from the binary, the result in decreasing of orbital radius is known as inspiral. When the black holes get close enough, they will merge into a single black hole. After the merge, any distortion will dissipate in form of gravitational waves, which is known as ringdown.

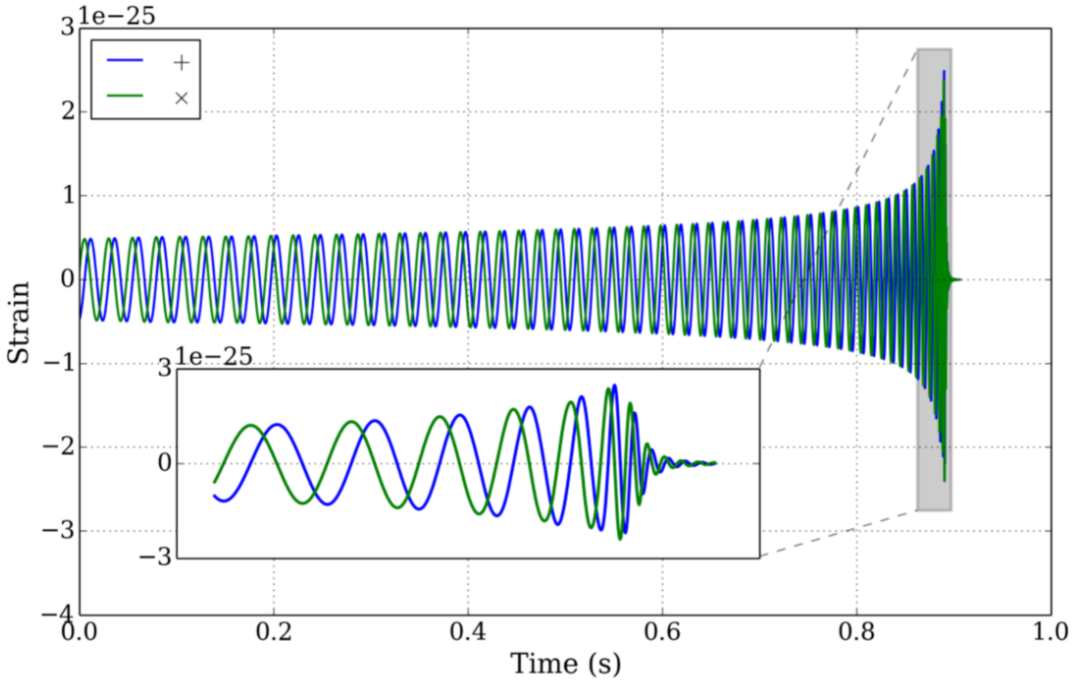

Figure 2: Impiral-Megrer-Ring-down Process[1].

4 gstlal pipeline

The search pipelines use matched filtering method to find the gravitational wave signals buried in noise. The search pipelines first compute signal-to-noise ratio (SNR) of the detector output with all the waveform templates in the bank of templates. If the SNR of the data is larger than some threshold, the potential signal is known as trigger. The matched filtering is the optimal method to find the signal if the signal is buried in stationary Gaussian noise. However, in LIGO data, the instrumental artifacts can produce non-stationary noise, which is known as glitches. The glitches can have a high SNR and cause a false alarm in analysis, a χ^2 veto is used to reject the false signals.

We aim to join gravitational wave observations with electromagnetic wave observations. The Low Latency Online Inspiral Detection (LLOID) algorithm is developed to achieve a low-latency search for gravitational waves. gstlal is a search pipeline to achieve a low-latency search for gravitational wave signals. The low-latency search pipeline uses in aLIGO can send out astronomical alert to the electromagnetic telescopes within a few minutes. In order to achieve the low-latency search, several technique is used to reduce the computational resource. A detailed explanation of the pipeline can be found in Ref. [2].

4.1 Matched filtering

Matched filtering is a method to extract the signals from a noisy data by comparing the detector output with a predicted waveform template. The matched filtering method the optimal filter to get the largest signal-to-noise ratio in stationary Gaussian noise. Consider the detector output signal $s(t) = n(t) + q(t)$ where $n(t)$ is the noise and $q(t)$ is the gravitational wave signal, we can compute the cross correlation between the detector output with a template h

$$c(\tau) = \int_{-\infty}^{\infty} s(t)h(t+\tau)dt. \tag{4.1.1}$$

We can transform it in to frequency domain, such that

$$c(\tau) = \int_{0}^{\infty} \tilde{s}(f)\tilde{h}^*(f)e^{2\pi i f\tau}df, \tag{4.1.2}$$

where $\tilde{s}(f)$ is the Fourier transform of $s(t)$ and $\tilde{h}^*_{\text{template}}(f)$ is the complex conjugate of the Fourier transform of $h(t)$. In order to whiten the signals, the correlation is weighted by the power spectral density $S_n(f) = \langle\tilde{n}(f)\tilde{n}^*(f')\rangle$ such that

$$x(\tau) = \int_{0}^{\infty} \frac{\tilde{s}(f)\tilde{h}^*(f)e^{2\pi i f\tau}}{S_n(f)}df. \tag{4.1.3}$$

Consider both the two polarizations of gravitational wave, the signal-to-noise ratio (SNR) can be defined as

$$\rho^2 = 4\int_{0}^{\infty} \frac{\tilde{s}(f)\tilde{h}^*(f)e^{2\pi i f\tau}}{S_n(f)}df. \tag{4.1.4}$$

4.2 Template bank

The gravitational wave signals of compact binary depend on at least fifteen parameters. The intrinsic parameters such as mass and spin affect the waveform, and most of the extrinsic parameters only affect the amplitude of detector output.

The coalescence signals are parameterized by a set of parameters continuously. Since we cannot construct infinite set of templates for the matched filtering, a finite set of templates are chosen to construct the bank of templates. The templates are chosen such that any possible signal will have an inner product ≥ 0.97 with at least one template in the template bank. The template bank is said to have a minimal match of 0.97[2]. In gstlal, the stochastic placement algorithm is used to constructed the template bank. A detailed explanation of the stochastic method can be found in Ref. [3].

Parameters	Symbols
component masses	m_1, m_2
component spin vectors, each having three components	$\vec{S}_1$, $\vec{S}_2$
sky position: right ascension and declination	α, δ
orientation of the binary relative to the line of sight: inclination and polarization angle	ι, ϕ
luminosity distance	D
coalescence phase	ϕ_{coal}
coalescence time	t_{coal}

Table 1: The compact binary parameter space. There are at least fifteen parameters required to specify the orbit of a compact binary (we have ignored parameters associated with eccentricity and the finite size of neutron stars). We refer to the parameters (1)-(8) as intrinsic parameters, while (9)-(15) are called extrinsic. Parameters (9)-(13) enter only in the overall amplitude of the signal, (14) can be maximized over analytically, and (15) can be efficiently searched over with an inverse Fourier transform[1].

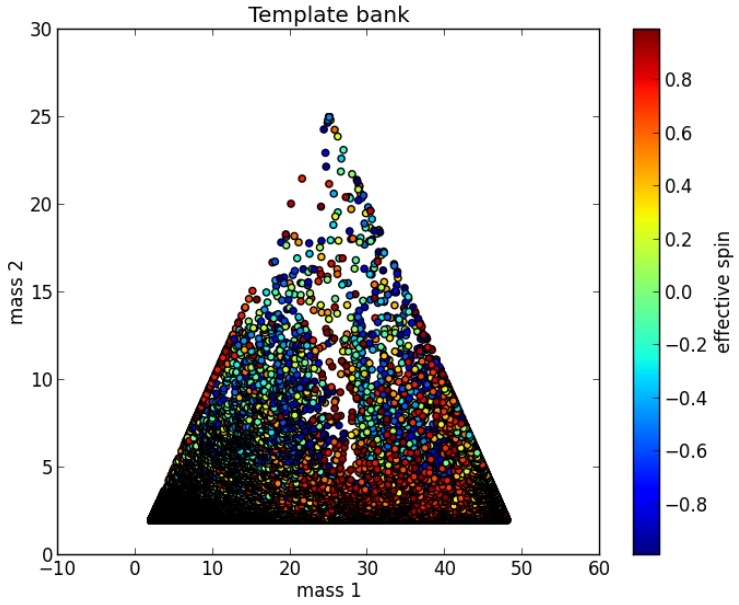

Figure 3: An example of template bank used in search pipeline with mass and effective spin shown in plot.

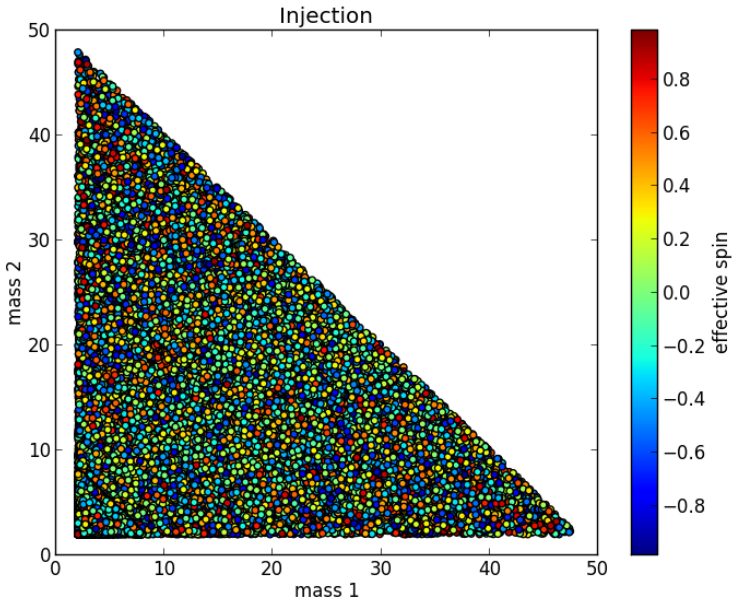

Figure 4: An example of SEOBNRv2 ROM DoubleSpin approx injection used in search pipeline with mass and effective spin shown in plot.

4.3 Transformations of templates

gstlal is a search pipeline designed to have a low-latency search. In order to reduce the computational cost, two transformations of the templates are used to produce orthogonal filters which is more computational efficient [2].

4.3.1 Multibanding

Nyquist frequency Nyquist frequency is the half of the sampling frequency f_s,

$$f = \frac{f_s}{2}. \tag{4.3.1.1}$$

The discretely sampled data with sampling rate f_s can completely represent a continuous signal which only has frequency content below the Nyquist frequency. The information of signal with frequency higher than the Nyquist frequency will be lost or aliased to lower frequency.

The beginning of the inspiral stage has a low frequency, a smaller sample rate is used to reduce the computational cost. The template is divided into time slices in time domain into multi-banding, each template $h_i[k]$ is decompose into a sum of S non-overlapping templates

$$h_i[k] = \sum_{s=0}^{S-1} \begin{cases} h_i^s[k] & \text{if } t^s \leq k/f^0 < t^{s+1} \\ 0 & \text{otherwise} \end{cases}, \tag{4.3.1.2}$$

for S integer $\{f^0 t^s\}$ such that $0 = f^0 t^0 < f^0 t^1 < \ldots < f^0 t^s = N$. The sampling frequency of each time slice must be smaller than Nyquist frequency. For the time-sliced template intervals $[t^0, t^1), [t^1, t^2), \ldots, [t^{S-1}, t^S)$ sampling at frequency $f^0, f^1, \ldots, f^{S-1}$ can be downsampled into

$$h_i^s[k] \equiv \begin{cases} h_i[k\frac{f}{f^s}] & \text{if } t^s \leq k/f^s < t^{s+1} \\ 0 & \text{otherwise} \end{cases}. \tag{4.3.1.3}$$

Downsampling reduces the total number of filter coefficients by a factor of ≈ 100 by treating the earliest part of the waveform at $\approx 1/100$ of the full sample rate. [2].

4.3.2 Singular Value Decomposition (SVD)

The templates in the template bank are highly similar, large number of templates demand a high computational resource. The SVD is a method to reduce the number of filters. The template can be factorized in form of

$$h_i^s[k] = \sum_{l=0}^{M-1} v_{il}^s \sigma_l^s u_l^s[k], \tag{4.3.2.1}$$

where $u_l^s[k]$ are the orthonormal basis templates and $v_{il}^s \sigma_l^s$ is the reconstruction matrix. The number of templates can be reduces from M to L^s by taking away the least important bases indicated by σ_l^s

$$h_i^s[k] \approx \sum_{l=0}^{L^s-1} v_{il}^s \sigma_l^s u_l^s[k], \tag{4.3.2.2}$$

SVD reduces the number of filters needed by another factor of ≈ 100. [2].

4.4 χ^2 veto

To reject the false alarm, χ^2 method is used to distinguish the true signals from glitches. χ^2 compares the detector output with the waveform template.

Consider the detector output signal $s(t) = n(t) + q(t)$ where $n(t)$ is the noise and $q(t)$ is the gravitational wave signal, and the template waveform $h(t)$. We divide the frequency range of integration into a finite

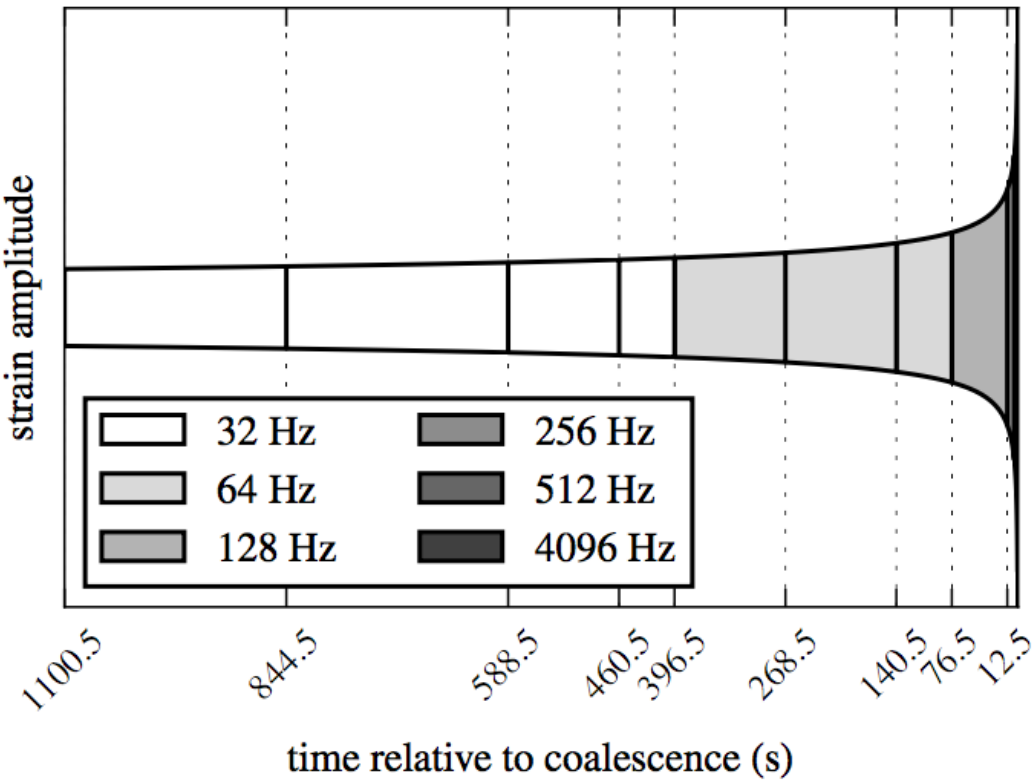

Figure 5: Multi-banding of templates. Different time slice using different sample rate increases the computational efficient.

number of bin $f_k \leq f \leq f_{k+1}$, where $k = 1, ..., p$. We define the contribution to the matched filtering statistic coming from the k-th bin by

$$z_k \equiv \langle h, x \rangle_k \equiv 2 \int_{f_k}^{f_(k+1)} \left[\tilde{h}^*(f)\tilde{x}(f) + \tilde{h}(f)\tilde{x}^*(f) \right] \frac{df}{S_n(f)}, \tag{4.4.1}$$

where $\tilde{x}(f)$ and $\tilde{h}(f)$ are the Fourier transform of $x(t)$ and $h(t)$ respectively, $\tilde{x}^*(f)$ and $\tilde{h}^*(f)$ is the complex conjugate of the Fourier transform of $x(t)$ and $h(t)$ respectively. If we sum over the matched filtering statistic from $f_1 = 0$ to $f_p = \infty$, it gives

$$z = \langle h, x \rangle \equiv 2 \int_0^\infty \left[\tilde{h}^*(f)\tilde{x}(f) + \tilde{h}(f)\tilde{x}^*(f) \right] \frac{df}{S_n(f)}. \tag{4.4.2}$$

We can construct the χ^2 as

$$\chi^2 = p \sum_{k=1}^{p} \left(z_k - \frac{z}{p} \right)^2. \tag{4.4.3}$$

A true signal looks similar with the template waveform, so it has a small χ^2. But for a glitch, the difference between the output and the template is large, therefore it has a large χ^2. We can use this method to separate the signal from noise and increase the sensitivity of the search pipeline.

5 Waveform of gravitational signals from coalescence of binary

In order to have a intuitive image of the gravitational wave signals, we have generate some waveforms in time domain and frequency domain using simulation. The parameters of the signal are varied to understand the effect of different parameters.

The strain amplitude of gravitational wave signals $h = \Delta L/L$ can be approximated by the quadrupole approximation

$$h \approx \frac{4\pi^2 G M a^2 f_{orb}^2}{c^4 r}, \tag{5.1}$$

where G is the gravitational constant, M is the mass of the star, a is the distance between the binary, c is the speed of light and r is the distance from the system to the observer.The energy loss in quadruple approximation is

$$\dot{E}_{GW} = -\frac{32}{5}\frac{G^4}{c^5}\frac{\mu^2 M^3}{a^5}, \tag{5.2}$$

where $M = m_1 + m_2$ is the total mass of the system, $\mu = \frac{m_1 m_2}{M}$ is the reduced mass and a is the orbital separation. These equations can help us to understand the feature of the waveform.

5.1 Varying the total mass of binary

Fig. 6a shows the time domain waveform with vary mass and fixed distance of 1Mpc. Obviously, for a higher mass system, the amplitude of strain is larger. As expected in Eq. 5.1, a more massive object is a stronger source of gravitational waves.

From Fig. 6a, a more massive system has a smaller chirp time. From Fig. 6a, a more massive system end the coalescence at a lower frequency. Consider Eq. 5.2, for a larger mass system, the energy loss due to gravitational radiation is larger. Therefore, a larger mass system will end the coalescence quicker with a lower frequency.

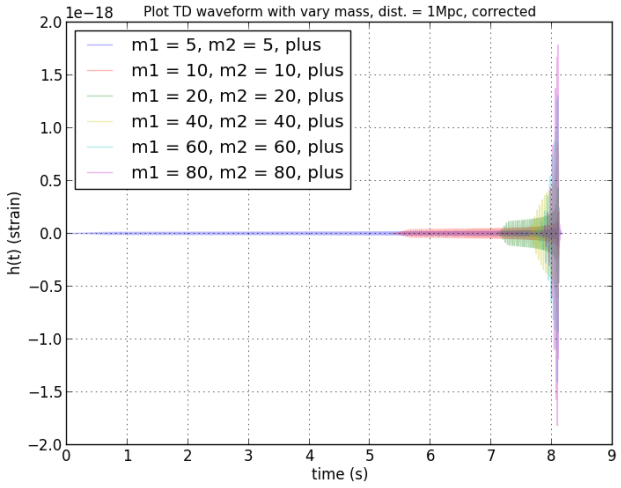

(a) The time domain simulated waveform SEOBNRv2 ROM DoubleSpin approx with varying total mass. Plus polarization is shown. Different waveforms are put together for comparison.

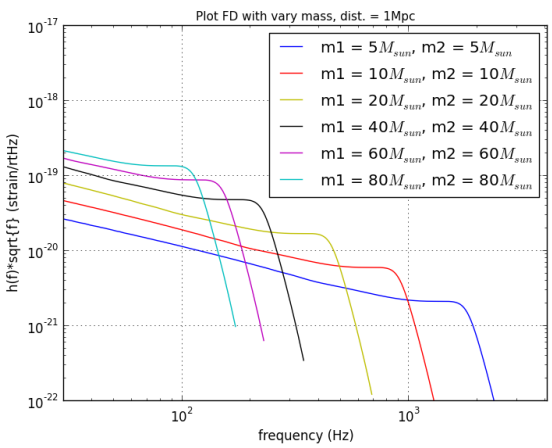

(b) The frequency domain simulated waveform SEOBNRv2 ROM DoubleSpin approx with varying total mass.

Figure 6: Time domain and frequency domain waveforms with varying mass.

5.2 Varying the mass ratio of binary

All the simulated waveform is set to have a total mass of $100M_{sun}$. Consider the reduced mass $\mu = (m_1 m_2)/M$, for the same total mass, if the system has a larger mass ratio, the reduced mass is smaller. Since the strain is proportional to the reduced mass, therefore, a larger mass ratio has a smaller strain.

From Fig. 7, a larger mass ratio system end the coalescence quicker with a lower frequency. By Eq. 5.2, the energy loss of the system due to the gravitational waves is proportional to the reduced mass. Therefore, a larger mass ratio system will end the coalescence quicker with a lower frequency.

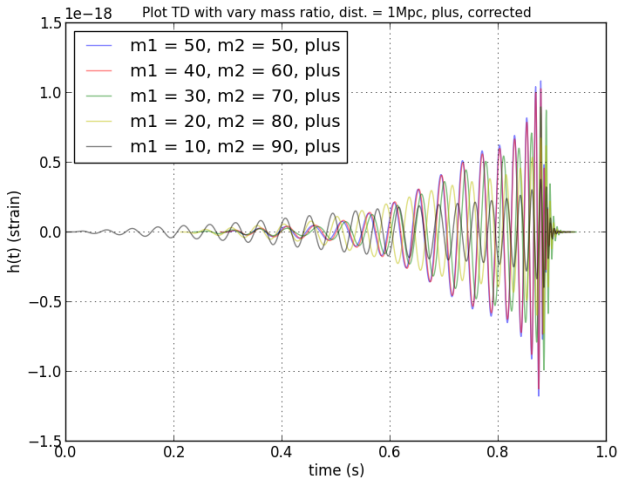

(a) The time domain simulated waveform SEOBNRv2 ROM DoubleSpin approx with varying total mass ratio. Plus polarization is shown. Different waveforms are put together for comparison.

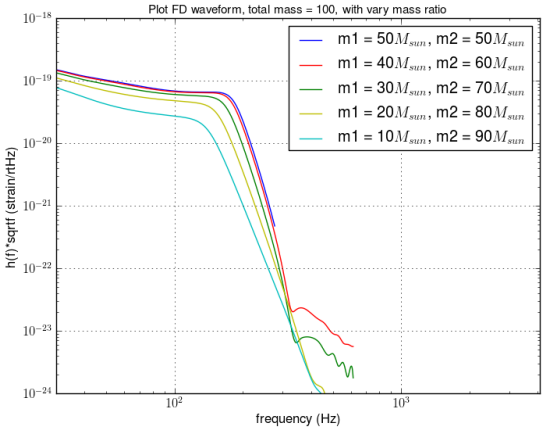

(b) The frequency domain simulated waveform SEOBNRv2 ROM DoubleSpin approx with varying total mass ratio.

Figure 7: Time domain and frequency domain waveforms with varying mass ratio.

5.3 Varying the distance from the source to observer

The strain of amplitude decreases with distance. Using Eq. 5.1, the strain h is inversely proportional to the distance r

$$h \propto \frac{1}{r}.$$

Therefore, a distant binary has a smaller strain.

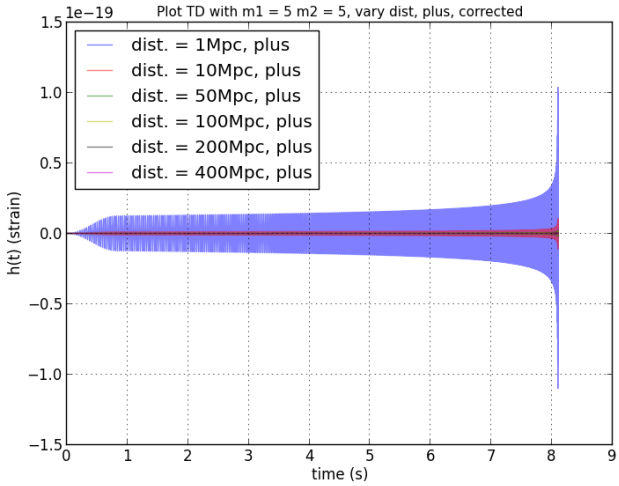

(a) The time domain simulated waveform SEOBNRv2 ROM DoubleSpin approx with varying distance. Plus polarization is shown. Different waveforms are put together for comparison.

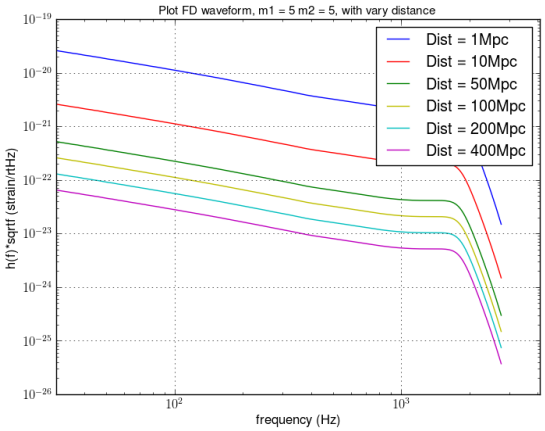

(b) The frequency domain simulated waveform SEOBNRv2 ROM DoubleSpin approx with varying distance.

Figure 8: Time domain and frequency domain waveforms with varying distance.

5.4 Varying the aligned spin

The spinning effect of the binary is parametrized by the effective spin

$$\chi_{\text{eff}} \equiv \frac{m_1\chi_1 + m_2\chi_2}{m_1 + m_2}, \tag{5.4.1}$$

where χ_1 and χ_2 are the dimensionless spins of binary objects.

Fig. 9a shows that for a larger spin, the time for coalescence is longer. Fig. 9b shows that a lager spin result a small increase of strain and the merger occurs at a lower frequency.

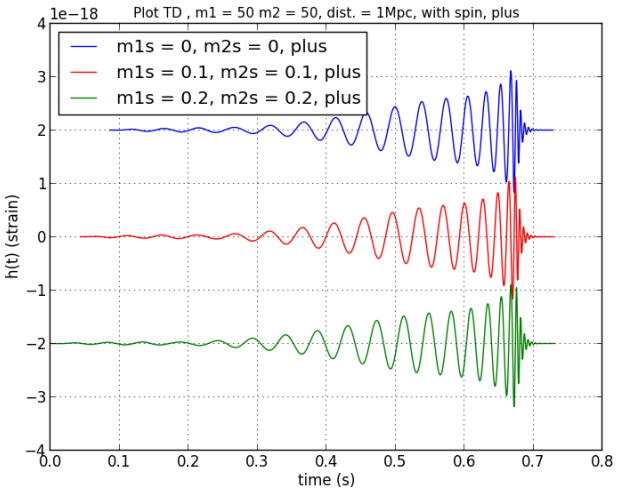

(a) The time domain simulated waveform SEOBNRv2 ROM DoubleSpin approx with varying spin. Plus polarization is shown. Different waveforms are put together for comparison.

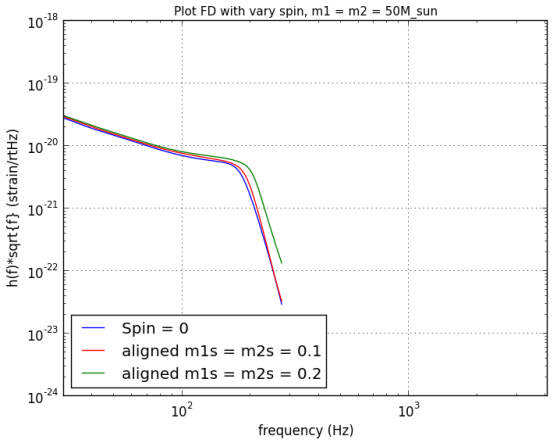

(b) The frequency domain simulated waveform SEOBNRv2 ROM DoubleSpin approx with varying spin.

Figure 9: Time domain and frequency domain waveforms with varying spin.

As shown in Fig. 10, when we oppose the spin of the binary, the time for coalescence and the strain will be smaller.

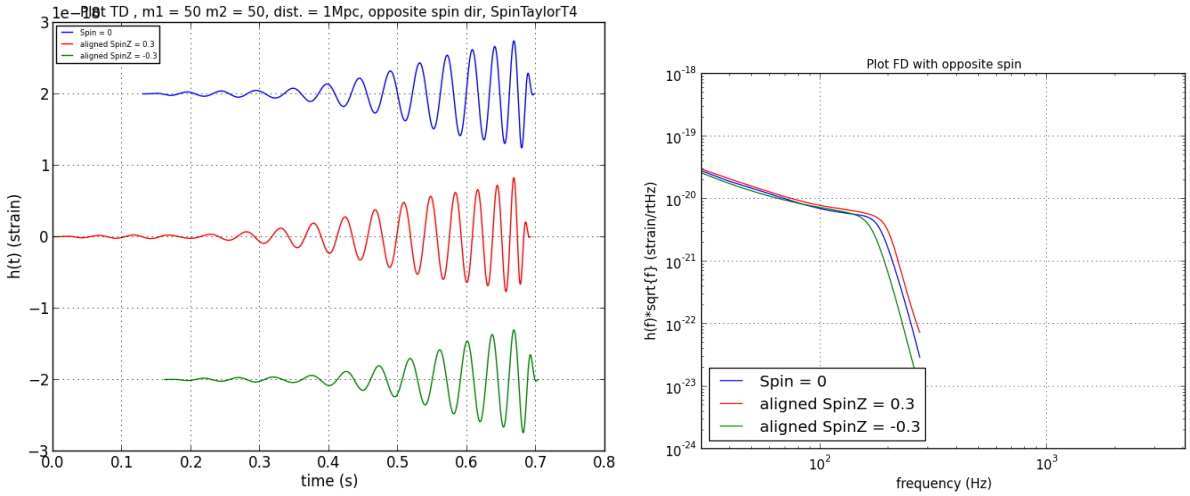

(a) The time domain simulated waveform SpinTaylorT4(b) The frequency domain simulated waveform SEOBNRv2 approx with opposite spin. Plus polarization is shown. Dif-ROM DoubleSpin approx with opposite spin. ferent waveforms are put together for comparison.

Figure 10: Time domain and frequency domain waveforms with opposite spin.

5.5 Precessing Spin

Apart from changing the spin parameters in z direction, we can change the spin parameters in both x, y and z direction. For processing spin, we can see the amplitude modulation effect.

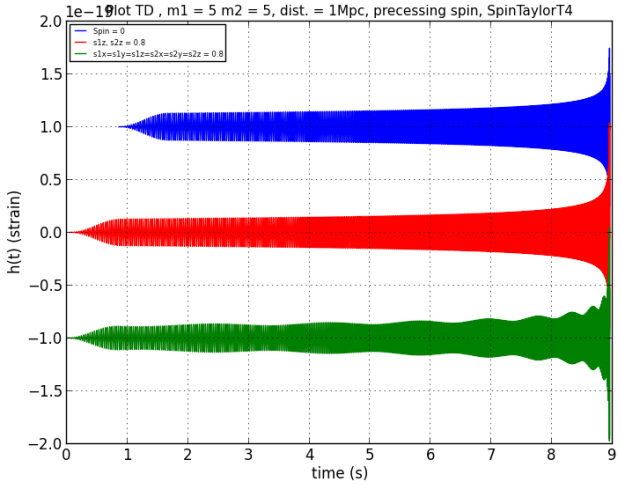

(a) The time domain simulated waveform SpinTaylorT4 approx with precessing spin.

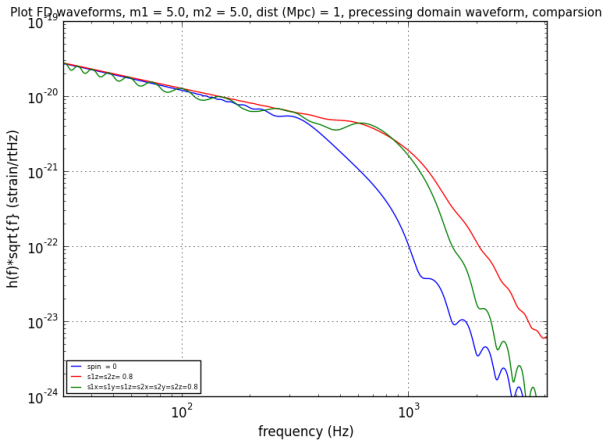

(b) The frequency domain simulated waveform SpinTaylorT4111 approx with precessing spin. Only inspiral part.

Figure 11: Time domain and frequency domain waveforms with precessing spin.

5.6 Comparing the time domain and the frequency domain

For the time domain plot, the strain amplitude of merger stage is largest, but the amplitude of merger frequency is small. It is because although the stain of inspiral part is small, it has a longer duration than the merger stage, therefore the amplitude of the frequency decrease with increasing frequency.

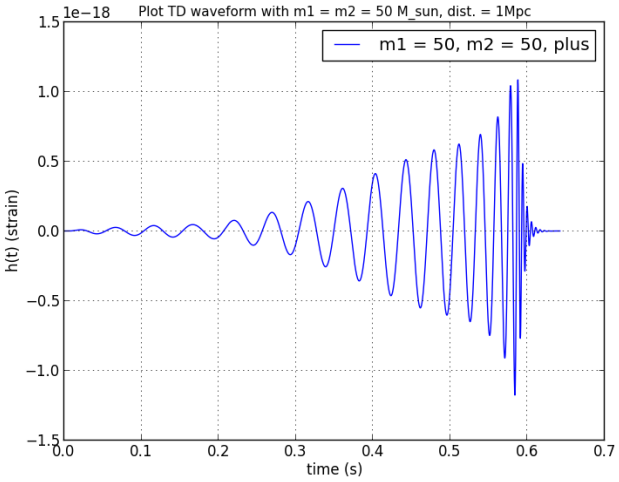

(a) The time domain simulated waveform SpinTaylorT4 approx with $m_1 = m_2 = 50M_{sun}$.

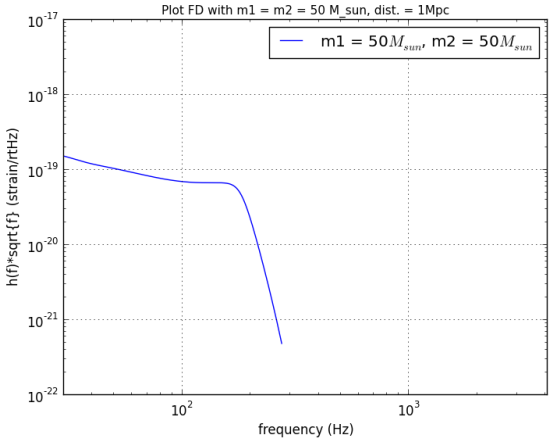

(b) The frequency domain simulated waveform SpinTaylorT422 approx with $m_1 = m_2 = 50M_{sun}$.

Figure 12: Time domain and frequency domain waveforms with $m_1 = m_2 = 50M_{sun}$.

5.7 ASD plot with aLIGO expected noise curve

The expected noise curve of aLIGO is plotted with the simulated waveform. The sensitivity of aLIGO is improved compare with iLIGO

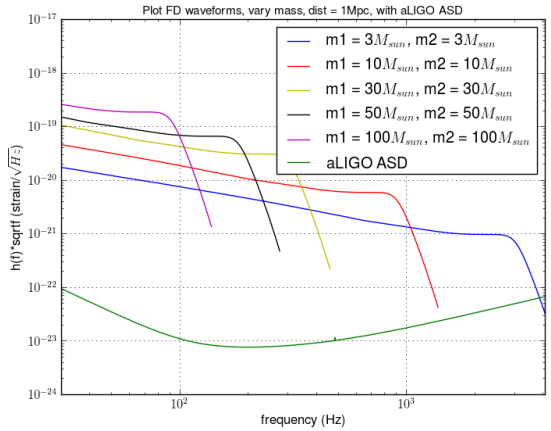

(a) The frequency domain simulated waveform SEOBNRv2 ROM DoubleSpin approx with vary mass. ASD of aLIGO is shown.

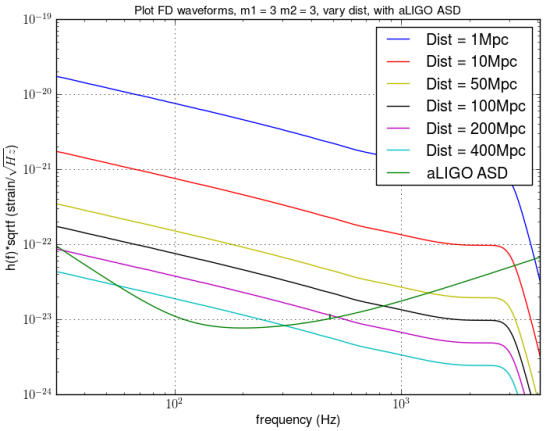

(b) The frequency domain simulated waveform SEOBNRv2 ROM DoubleSpin approx with opposite spin.

Figure 13: Time domain and frequency domain waveforms with opposite spin.

The expected noise curve of aLIGO is used to calculate the maximum distance that the coalescence signal can reach a SNR value of 8. The high mass binary coalescence can be detected by aLIGO since the seismic noise is greatly suppressed, the signal in low frequency range can be detected. The plot shows that the sensitivity of aLIGO is much better than that of iLIGO.

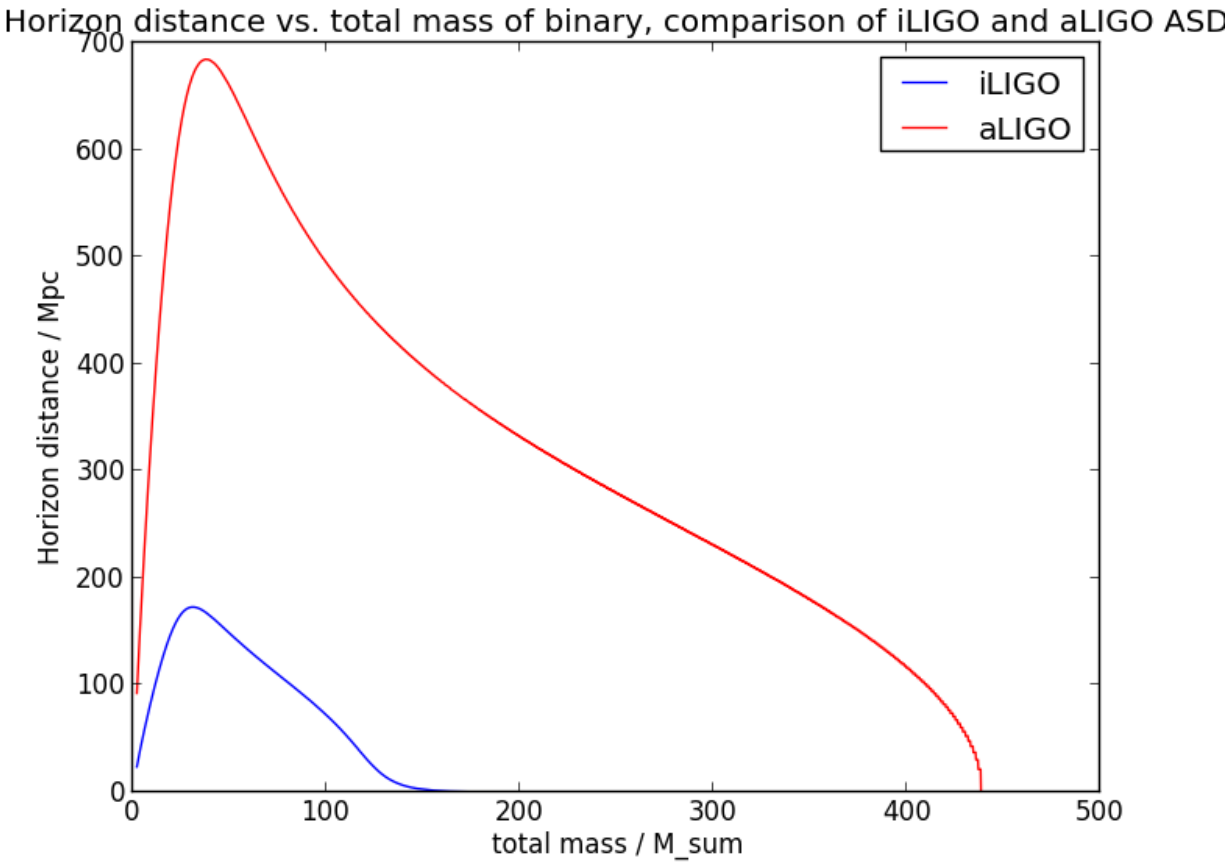

Figure 14: Horizon distance vs. total mass, comparison between iLIGO and aLIGO. The sensitivity of aLIGO has been improved.

6 Machine Learning

A trigger, which is a signal candidate, contains a set of parameters such as signal-to-noise ratio, different types of χ^2, chirp mass and spin. We would like to train our computer to identify whether the trigger is a true signal or not when it has this set of parameters. Moreover, other than the parameters considered in the pipeline, some factors can also be taken in consideration in identifying the signals, such as the time difference between two detectors when they have formed a coincident. Our pipeline model may not have considered all the factors which can affect the classification between signal and noise, we would like to use some method to consider as many factors as we can to identify the signal.

A computational technique called machine learning can be used to train the computer to do the classification. In this project, we are going to inject the simulated signals into the search pipeline and get a set of parameters for each trigger, then we will do a supervised learning to train the computer to classify the trigger from signal to noise.

6.1 Machine learning and search pipeline

Machine learning is to learn from data.

	The essence of machine learning
1	A pattern exist.
2	We cannot pin it down mathematically.
3	We have data on it.

We are going to classify the triggers into real gravitational wave signals and noise. A real signal has a different set of parameters from a noise, a pattern exist such that we can try to find the underlying pattern between true signals, noise and the parameters through learning. Besides, it is difficult to analytically write down a equation that relates the classification and the parameters, this leads to the help of computer. Moreover, we can simulate waveforms and the parameters can be found through injection to the pipeline, this allows us to use the simulation data to train the computer. Based on these properties, we are going to use machine learning to reduce the false alarm rate and optimize the sensitivity of search pipeline.

The elements in machine learning:

- **Unknown target function** $f : X \to Y$
- **Input N set of data**
  $(\mathbf{x}_1, y_1), \ldots, (\mathbf{x}_N, y_N)$, where $\mathbf{x} = (x_1, \ldots, x_d), \mathbf{x} \in X, y \in Y$
- **Hypothesis set (Learning model)** $\mathbb{H}$
  $h_1, \ldots, h_M \in \mathbb{H}$
- **Best hypothesis**
  $g \approx f$, where $g \in \mathbb{H}$
- **Learning algorithm** λ

6.2 Feasibility of learning

We are going to use finite set of data for the classification learning. The hypothesis found using the in-sample data can have a good performance with the in-sample data, but there is no guarantee that the hypothesis preforms good outside the data. In order to generalize the learning from the in-sample data to out of sample data, a theory is required to ensure the learning is probable outside the sample data. It is important for us because the theory can guarantee that the model found using the data from simulation can also be used in real situation.

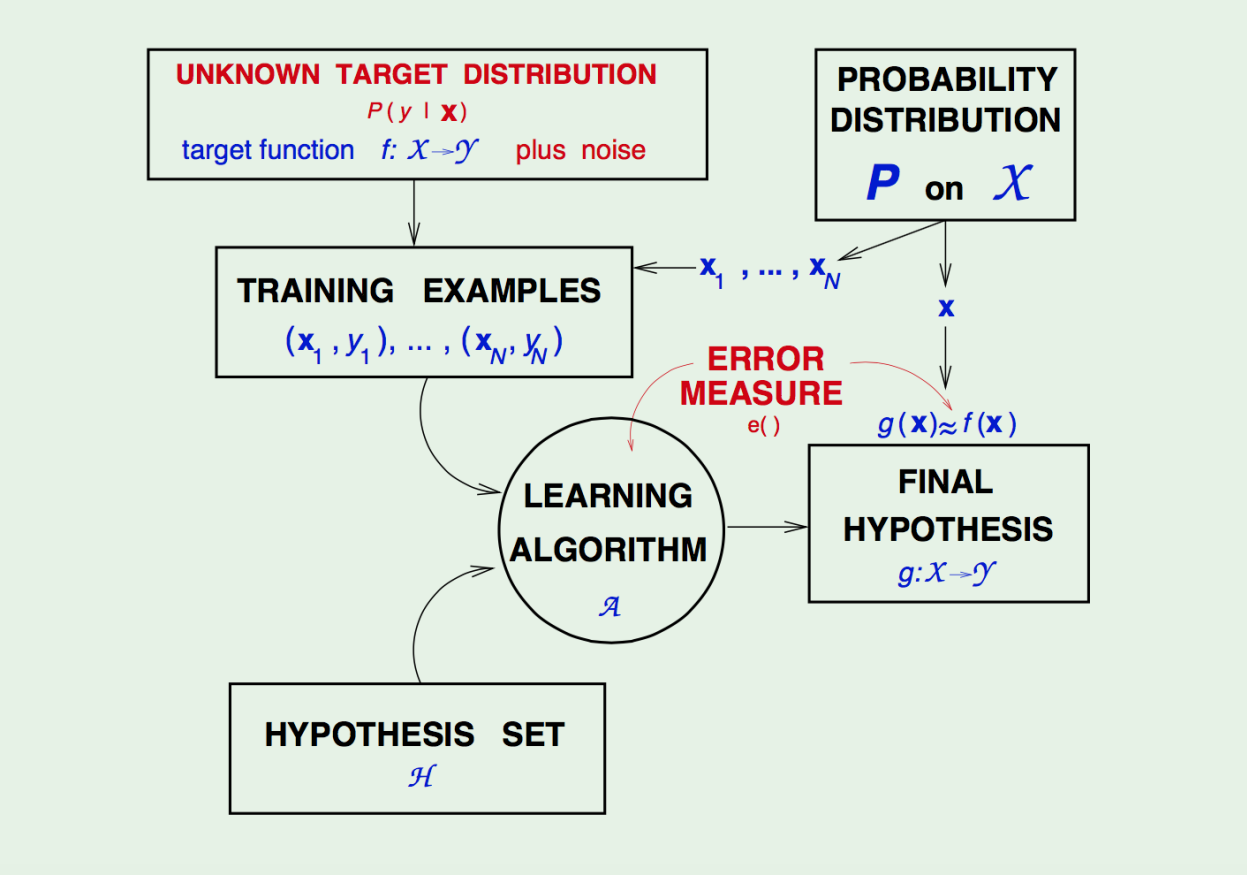

Figure 15: Learning diagram[4].

Vapnik-Chervonenkis Inequality (VC inequality) stated that the probability of the difference between the error of in-sample data and the target function E_{in} and the error of out of sample data and the target function E_{out}, which less than a value ϵ, is bounded by

$$P\left[|E_{\text{in}}(g) - E_{\text{out}}(g)| > \epsilon\right] \leq 4m_{\mathbb{H}}(2N)e^{-\frac{1}{8}\epsilon^2 N}, \tag{6.2.1}$$

where N is the number of in-sample data, and

$$m_{\mathbb{H}}(2N) = \sum_{i=0}^{d_{VC}} \binom{2N}{i}, \tag{6.2.2}$$

where d_{VC} is a quantity depends on the hypothesis set which measure the complexity of the hypothesis set. $m_{\mathbb{H}}(2N)$ is a polynomial with maximum power of $N^{d_{VC}}$. The right hand side of the VC inequality contains a decay exponential term. Since exponential increase faster then polynomial, which can be proved by doing $b+1$ times L'Hoptial's rule

$$\lim_{n\to\infty} \frac{n^b}{a^n} = 0, \tag{6.2.3}$$

the probability will bound by a value less than one when the number of data N increase to certain amount. Therefore, machine learning is feasible for improving the sensitivity of search pipeline.

Example of machine learning

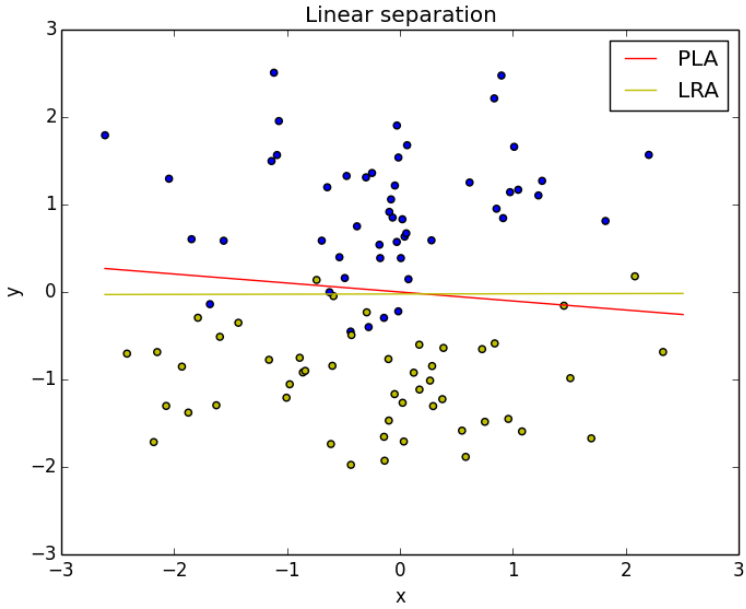

Figure 16: A comparison between perceptron learning algorithm and linear regression algorithm.

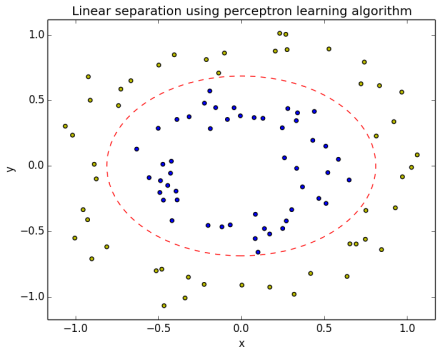

(a) Circular separated data point. A non-linear transformation is used.

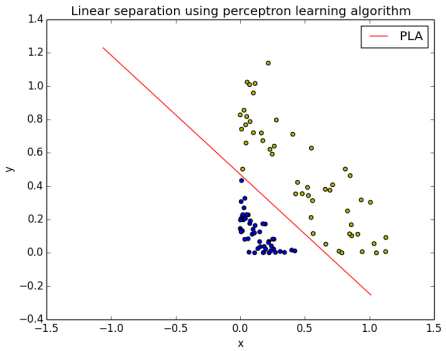

(b) The data becomes linearly separable after the transformation.

Figure 17: The data is separate in circular sequence. The data is not linearly separable. A non-linear transform is used in tackling the problem. The data $\mathbf{x}$ is transformed from (x_1, x_2) into (x_1^2, x_2^2). It is measuring the distance of the data point from the centre. After the transformation, the data becomes linearly separable and the perceptron learning algorithm can be used.

6.3 Future work

I have studied some simple models and learn the theory behind machine learning. I am going to construct a neural network for the classification and learn different algorithm that can be used in this project.

7 Plan

Date	Task
Now to the end at Caltech	
6th July - 10th July	Attend Caltech Gravitational Wave Astrophysics School (CGWAS).
7th July - 19th August	Learn different model of machine learning.
7th July - 2nd August	Begin to run high-statistics simulation and evaluate the pipeline sensitivity.
20th July - 23rd July	Visit LIGO at Livingston.
20th July - 20th August	Work on machine learning to improve the sensitivity of search pipeline.
24th July - 2nd August	Work on second progress report and the abstract of final report.
3rd August	**Progress Report II**
3rd August	**Abstract**
3rd August - 19th August	Prepare the final presentation and the final report.
20th August	**Oral Presentation**
After Research	
25th September	**Final Report**

References

[1] Privitera, Stephen M., (2014), *The importance of spin for observing gravitational waves from coalescing compact binaries with LIGO and Virgo.* Dissertation (Ph.D.), California Institute of Technology. http://resolver.caltech.edu/CaltechTHESIS:05282014-160218103

[2] K. Cannon et. al., *Toward Early-warning Detection of Gravitational Waves from Compact Binary Coalescence*, ApJ. **748** (2012) 136, [arXiv:1107.2665v4].

[3] I. W. Harry, B. Allen, and B. Sathyaprakash, *A stochastic template placement algorithm for gravitational wave data analysis*, Phys. Rev. D **81**, 024004 (2009), 0908.2090, [arXiv:0908.2090].

[4] Y. S. Abu-Mostafa, (2012). *Machine Learning* [PowerPoint slides]. Retrieved from http://work.caltech.edu/lectures.html

[5] R. A. Hulse and J. H. Taylor, *Discovery of a pulsar in a binary system*, Astrophys. J., Lett. **195**, L51 (1975).